Pergamon

Cement and Concrete Research 32 (2002) 881–891

CEMENT AND CONCRETE RESEARCH

Impedance spectroscopy study of hardened Portland cement paste

M. Cabeza[a], P. Merino[a], A. Miranda[b], X.R. Nóvoa[a,*], I. Sanchez[a]

[a]*Universidade de Vigo, E.T.S.E.I.M., Lagoas-Marcosende 9, E-36200 Vigo, Spain*
[b]*NORCONTROL S.A., Carretera NVI Km 582, 15168 Sada (A Coruña), Spain*

Received 17 January 2001; accepted 14 December 2001

Abstract

In this paper, the differential impedance analysis (DIA) has been applied to the study of the dielectric properties of hardened Portland cement paste. Two time constants are found in the impedance spectra obtained in the frequency region form 100 kHz to 15 MHz. One time constant has been attributed to the solid matrix and the other one to the liquid phase filling the pores. The effect of the cement paste–electrodes interface has been quantified using two different experimental set-ups. Measurements using direct contact between electrodes and cement paste have been compared with measurements using an air gap technique in which the specimen ''floats'' between the electrodes. The two referred time constants have been found in both types of measurements. The influence of drying on the dielectric parameters is also studied.

Keywords: Characterization; Electrical properties; Cement paste; Impedance spectroscopy (IS); Differential impedance analysis (DIA)

1. Introduction

Impedance spectroscopy (IS) studies on concrete, mortar and cement paste have been conducted initially due to the possibility of correlating the material dielectric and mechanical properties [1,2]. Even if recent studies [3] claim for the possibility of obtaining cement paste dielectric constants at frequencies below 200 kHz, it has been demonstrated that the dielectric response appears at frequencies above this one [4,5]. It is in the kilohertz-frequency range and below where the electrode–electrolyte interface (dominated by the double-layer capacitance), the redox phenomena developing at the electrodes, and the transport phenomena from and to the electrolyte bulk are measured [6].

As stated in a previous work [4], the identification of the number of time constants present in the high-frequency range of the impedance spectra is the key question. Some work in this field considered the high-frequency loop as only due to the dielectric response of the material [7–10], an assumption leading to dielectric constant values higher than 10^3, very far from the typical ones found for ceramic materials [11]. These high dielectric constant values were explained using a Dielectric Amplification Factor (DAF) [8,9].

More recent studies by the authors considered two contributions in the high-frequency region of the impedance spectra, one due to the solid phase [4,5] and a second one probably due to the ionic motion of free ions in the electrolyte filling the pores [12]. This approach allowed to obtain dielectric constant values close to the typical for ceramic materials, thus, any DAF was not necessary to interpret results.

Concerning the analysis of impedance data, Stoynov et al. [13–16] presented the differential impedance analysis (DIA) as a technique to determine the number of time constants present in an impedance spectrum, without any consideration about the model involved. In the present paper, this technique has been applied to determine the time constants contributing to the high-frequency region of the impedance spectra.

This paper is organised as follows. The Experimental section concerns the preparation of cement specimens as well as the methodology employed. The basics of the DIA method, fitting procedure, and Kramers–Kroning (KK) test are introduced in the Data processing section. The Results and discussion section reports IS results using contacting and air gap techniques. The dielectric constant of the cement paste is calculated for the two methods and the obtained values are discussed. Finally, the influence of drying in the dielectric parameters is studied.

* Corresponding author. Tel.: +34-986-81-22-13; fax: +34-986-81-22-01.
E-mail address: rnovoa@uvigo.es (X.R. Nóvoa).

0008-8846/02/$ – see front matter
PII: S0008-8846(02)00720-2

2. Experimental

2.1. Specimens

Portland cement CEMI52.5R according to the Spanish standard UNE 80303:96 was employed for the sample preparation. The mixtures have been prepared using three different water-to-cement ratio (0.4, 0.5 and 0.55). The mixtures have been cast into cylindrical moulds of 5.9 cm diameter and 20 cm height, and cured at 100% RH for 15 days. After the initial curing period, slices of thickness ranging from 3 to 9 mm were cut from the original cylinders and reintroduced in the curing chamber up to a total curing time of 28 days before starting measurements.

2.2. Measuring techniques

IS in the frequency region 15 MHz down to 10 kHz was used. The equipment employed to obtain the impedance spectra was a HP4194A Impedance/Gain-Phase analyser. This apparatus allows capacitance measurements in the range of 10^{-14} to 0.1 F having a maximum resolution of 10^{-15} F.

The specimen's impedances have been measured by two different methods: a contact method that uses graphite flexible electrodes firmly in contact with the specimen as shown in Fig. 1A, and a noncontacting method based in the HP16451B Dielectric Test Fixture. In this method, an air gap of 100 μm at each side of the specimen (Fig. 1B) avoids any contribution of the electrode–specimen interface in the measurement. The effective electrode surface area was, in this case, 11.34 cm^2. The impedance of the air gaps was measured prior to the bulk measurement and numerically subtracted so that this difference corresponds to the impedance of the cement paste without interfacial contributions.

For the contacting method, impedance measurements are possible in the frequency range 100 Hz up to 40 MHz, while in the noncontacting one, the upper limiting frequency is 15 MHz.

3. Data processing

3.1. KK validation

The KK relations connect the real and imaginary parts of a complex function of a real variable. Given a complex function of a real variable ω, $Z(\omega)=Z'(\omega)+jZ''(\omega)$, where $Z'(\omega)$ and $Z''(\omega)$ represent respectively the real and imaginary parts of the $Z(\omega)$ function, and $j=\sqrt{-1}$ The KK relations for this function can be expressed as follows [17]:

$$Z'(\omega)-Z'(0)=\left(\frac{2\omega}{\pi}\right)\int_0^\infty\left[\left(\frac{\omega}{x}\right)Z''(x)-Z''(\omega)\right]\times\frac{1}{x^2-\omega^2}\,dx \tag{1a}$$

$$Z''(\omega)=-\left(\frac{2\omega}{\pi}\right)\int_0^\infty\frac{Z'(x)-Z'(\omega)}{x^2-\omega^2}\,dx \tag{1b}$$

$$\theta(\omega)=\int_0^\infty\frac{\ln|Z(x)|}{x^2-\omega^2}\,dx \tag{1c}$$

In the particular case of an impedance spectrum, the variable ω is the angular frequency, and x is the auxiliary variable, having the same dimension as ω and varying between 0 and ∞. Thus, the measurement can be validated for causality, linearity and stability using one of these equations. Causality meaning the response of the system is due only to the perturbation (ΔV or ΔI) applied; linearity which means that the impedance is independent of the amplitude of the perturbation; and stability meaning the system returns to its original state after the perturbation is removed.

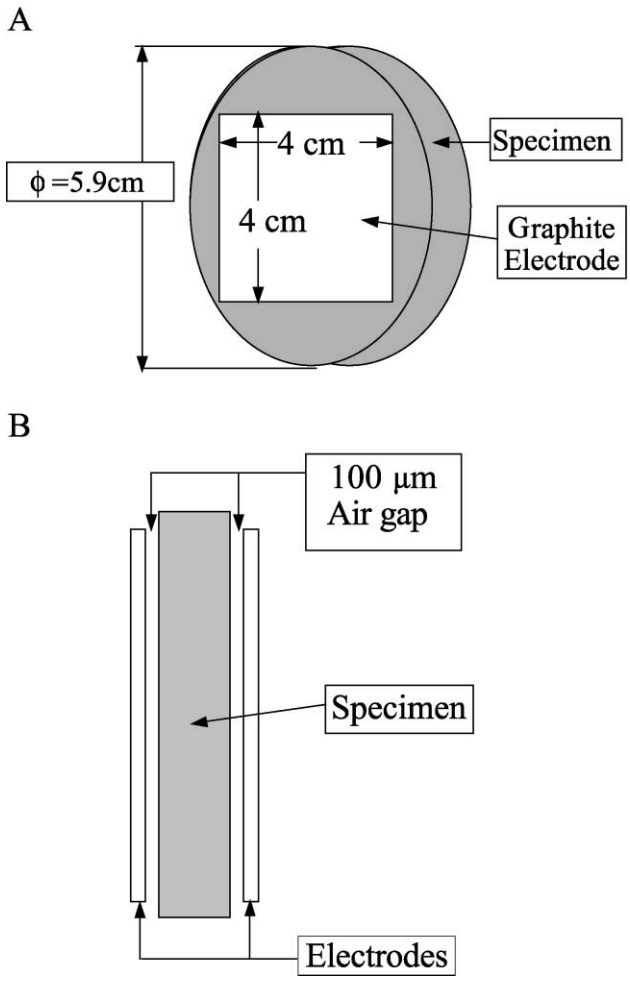

Fig. 1. (A) Side view of the electrode arrangement employed to perform measurements with direct contact between the driven electrodes and the specimen under test. (B) Side view of the electrode arrangement employed to perform measurements without direct contact between the driven electrodes and the specimen under test.

The KK relations have also been proposed as a "stability" criterion for the concrete [18], but the concept of stability employed in the referred paper is totally different from the above-defined one and has no a theoretical background.

Using the real or the imaginary part of the measurement, respectively, the imaginary (Eq. (1b)) or the real (Eq. (1a)) parts of the impedance spectra can be reconstructed using KK relations. If the impedance has been properly measured, the reconstructed impedance has to be equal to the measured values. All measurements performed in this study have been checked for KK consistency with a satisfactory result, as depicted in Fig. 2.

The application of Eqs. (1a)–(1c) requires the existence of a low-frequency limit of the impedance. To overcome this and other related difficulties, several solutions have been proposed in the literature. A good analysis of those problems can be found in Ref. [19].

3.2. Fitting procedure

The impedance data measured are fitted to an electrical circuit in which the different components have a physical meaning. The best fitting parameters of the circuit are obtained using a Simplex minimization method referred elsewhere [4]. The function to minimize, χ^2 in Eq. (2), includes the differences between the measured impedance and the calculated with the circuit model for every frequency.

$$\chi^2 = \sum_{i=1}^{N} \left[\left(\frac{a_{e_i} - a_{c_i}}{0.01|Z_{e_i}|} \right)^2 + \left(\frac{b_{e_i} - b_{c_i}}{0.01|Z_{e_i}|} \right)^2 \right] \quad (2)$$

In Eq. (2), N is the number of scanned frequencies, a_{e_i} and b_{e_i} correspond to the real and imaginary part of the impedance measured at the frequency f_i, and a_{c_i} and b_{c_i} are the real and imaginary part of the calculated impedance at the frequency f_i using the chosen model.

As can be deduced from Eq. (2), the experimental error is considered as 1% of the impedance modulus. A fitting factor quality q can be defined as (Eq. (3)):

$$q = \sqrt{\frac{\chi^2}{2N - N_p}} \quad (3)$$

where N_p is the number of the parameters calculated in the minimization of the error function. The quality of the fitting increases as q decreases.

3.3. Differential impedance analysis

This technique proposed by Stoynov et al. [13–16] is based on the point that the ratio $(dL_{eff}(\omega))/(dZ'(\omega))$, where $L_{eff}(\omega) = -(Z''(\omega))/(\omega)$, corresponds to the value of the time constant, $T(\omega)$ for the angular frequency at which the derivative is calculated (Eq. (4)).

$$T(\omega) = \frac{dL_{eff}(\omega)}{dZ'(\omega)} \quad (4)$$

A parallel RC circuit is the simplest case as $T(\omega) = RC$ for every frequency. In more complex systems, the value of the derivative is different for each frequency and some data processing is necessary to get the time constants involved.

The derivative is calculated numerically, and thus, a large number of data points are required. To obtain the necessary data points, a cubic spline interpolation is usually performed on the measured data [20]. The choice of this type of interpolation is to ensure that the first derivative is smooth, and the second derivative is continuous.

The application of Eq. (4) allows obtaining a set of data $f_i - T_j$ ($f_i = \omega_i/2\pi$) that can be directly represented in a $\log(f_i)$ vs. $\log(T_j)$ plot, as shown in Fig. 3A and B. In the simple case of a parallel RC circuit, $T_j = RC$ for every f_i (Fig. 3A), and for two RC, there is a frequency domain where $T_j = R_1C_1$ and, after a small transition zone, $T_j = R_2C_2$ (Fig. 3B). The frequency interval corresponding to the transition zone increases as the difference between the tow time constants values present in the spectrum decreases.

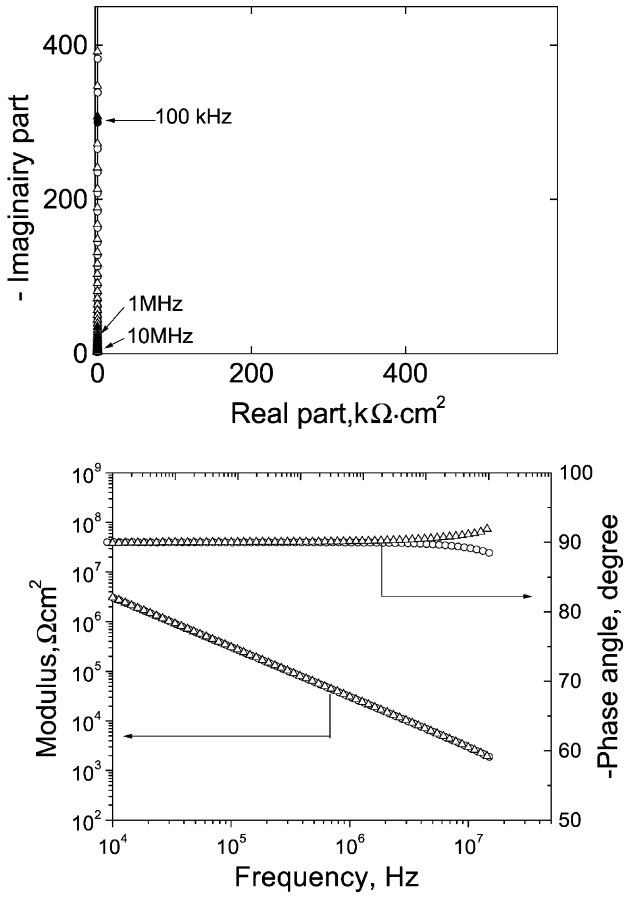

Fig. 2. Typical complex plane impedance plot (top) and Bode impedance plot (bottom). Experimental data (open dots) and their KK transform using Eq. (1b) (triangles).

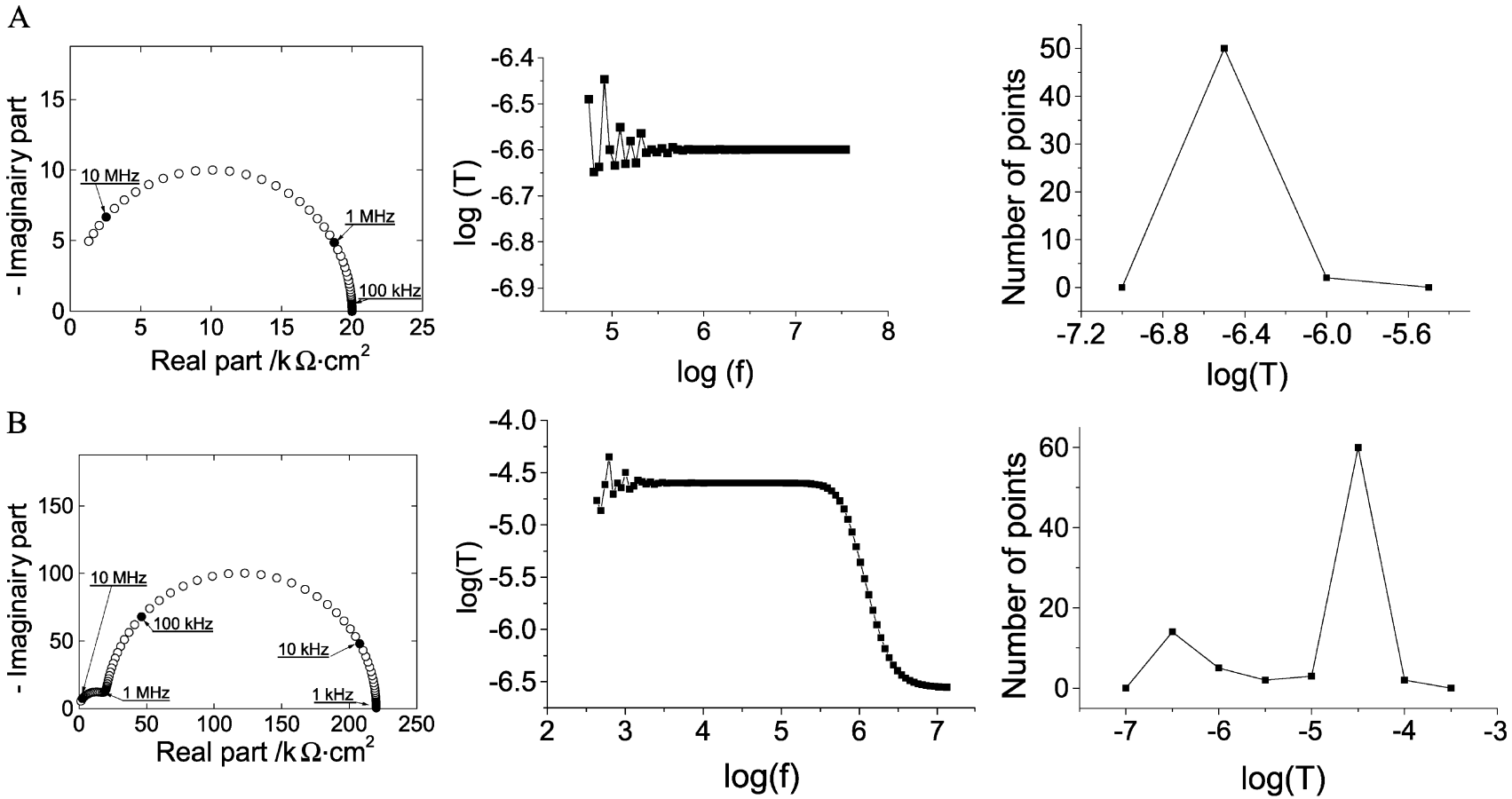

Fig. 3. (A) Complex plane impedance plot corresponding to an *RC* parallel arrangement $R = 20\ \text{k}\Omega$ and $C = 2$ pF (thus $T = RC = 40$ ns). The corresponding DIA representations are also depicted. (B) Complex plane impedance plot corresponding to two parallel *RC* elements coupled in series $R_1 = 20\ \text{k}\Omega$ and $C_1 = 2$ pF (thus $T_1 = R_2C_2 = 40$ ns); $R_2 = 200\ \text{k}\Omega$ and $C_2 = 20$ pF (thus $T_2 = R_2C_2 = 4\ \mu$s). The corresponding DIA representations are also depicted.

A more effective results representation is a time constant spectrum, also depicted in Fig. 3A and B. If the amplitude of each spectral line is chosen as ΔT, the number of time constants T_j complying with $T_i \leq T_j \leq T_i + \Delta T$ is the height (N_i) of the spectral line corresponding to T_i. The maxima of the plot N_i vs. log(T_i) correspond to the time constants of the system, as can be seen in Fig. 3A and B.

4. Results and discussion

4.1. Impedance measurements with/without contact sample/driving electrodes

Typical impedance diagrams for both types of measurements are given in Fig. 4A and B. For contacting electrodes

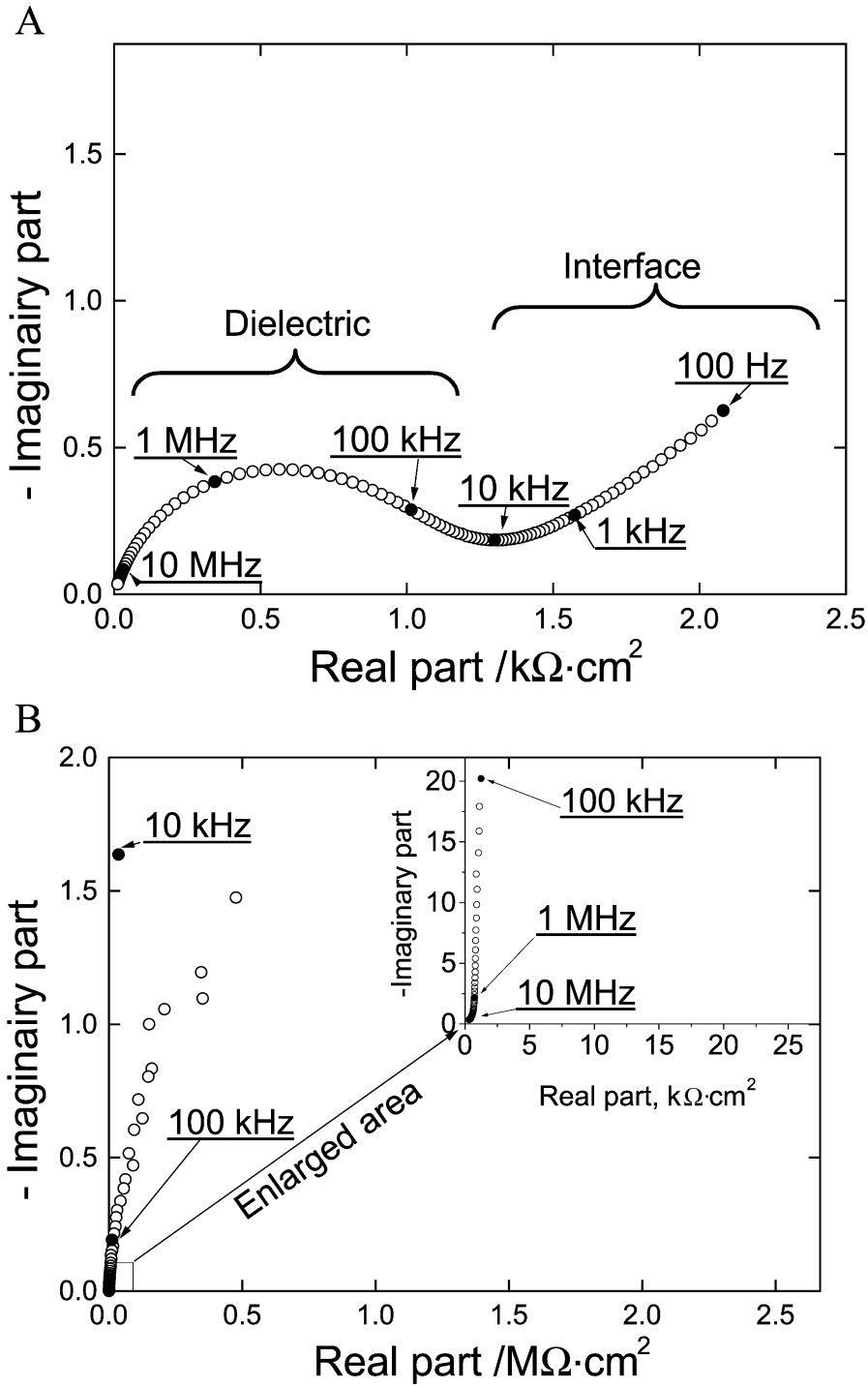

Fig. 4. (A) Experimental impedance data obtained on a w/c = 0.5 cement paste sample using the contacting method. The specimen thickness is $d = 0.4$ cm. (B) Complex plane impedance data as for (A) but using the noncontacting method.

(Fig. 4A), two capacitive loops are observed in the scanned frequency domain: the loop above 100 kHz representing the dielectric response of the system; and the queue below this frequency due to the cement–electrode interface contribution [2,4].

The impedance diagram for the noncontacting method (Fig. 4B), shows an almost pure capacitive behaviour in the high-frequency region (Fig. 4B, insert). Below about 10 kHz, the impedance values are higher than the instrument's measuring range and scattered data are obtained.

The feature of the complex plane impedance spectra as given in Fig. 4B has been modelled [5] using the equivalent circuit depicted in Fig. 5A where C_1 accounts for the dielectric capacitance associated to the solid phase, while C_2 and R_2 are related to ionic motion in "noncrossing pores" or regions internal to the sample.

In the present paper, only the "dielectric" part of the impedance spectra ($f > 100$ kHz), as given in Fig. 4A, is considered. A parallel resistance, R_1, has been added to the equivalent circuit depicted in Fig. 5B that accounts for the resistive behaviour observed. R_1 is related to ionic motion in "crossing pores" or regions external to the sample, in direct contact with the driving electrode.

Recently [21], a distribution of time constants in the frequency range 12 to 50 MHz for early age aluminous cement has been considered, however, the authors do not go further into details concerning the origin of this distribution. In order to give an insight into this aspect and verifying our previous hypotheses concerning the microstructure of this region of the impedance spectra [4,5], a DIA has been performed on the experimental data.

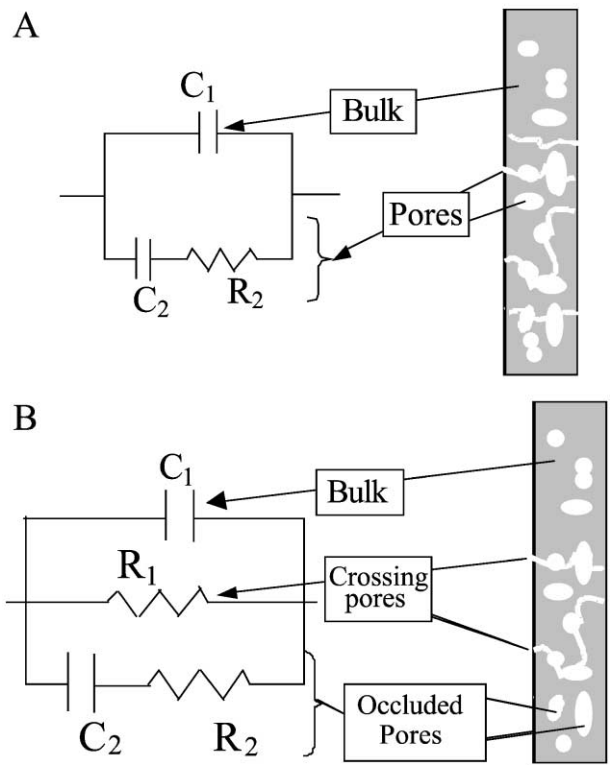

Fig. 5. (A) Equivalent circuit employed to model the data from the noncontacting method. (B) Equivalent circuit employed to model the data from the contacting method.

4.2. Differential impedance analysis

DIA is a powerful technique to identify the time constants present in impedance spectra without assuming any model for the system behaviour [13–16]. The data from 10 kHz to 15 MHz of the impedance measurement are analysed using this technique.

Fig. 6 illustrates the kind of results obtained. The histogram of $\log(T)$ corresponds to the high-frequency data given in Fig. 4A (contacting method). It is clear that the presence of two maxima in the plot corresponds to two time constants present in this frequency domain.

A convolution process can be undertaken in Fig. 6 to get the exact position of both maxima. The convoluted Lorentzian curves, also depicted in this figure, allow obtaining $\log(T_1) = -6.8$ and $\log(T_2) = -5.7$. This time constant values correspond to those obtained if the experimental data are modelled using two Voigt elements [22].

Thus, the results obtained from DIA confirm that two time constants are present in this domain of the impedance spectra.

4.3. Model parameters

In Section 4.1, the physical meaning of the equivalent circuits given in Fig. 5A and B has been introduced. This section is devoted to the discussion concerning the parameter values.

Eq. (5) corresponds to the impedance of the circuit model given in Fig. 5A. In this equation, the α_i parameter accounts for a Cole–Cole dispersion of the R_iC_i time constants.

$$Z(\omega) = R_0 + \frac{Z_1 Z_2}{Z_1 + Z_2}$$

$$\text{where } \left(Z_1 = \frac{R_1}{1 + (j\omega R_1 C_1)^{\alpha_1}} \right.$$

$$\left. \text{and } Z_2 = R_2 (1 + (j\omega R_2 C_2)^{-\alpha_2}) \right) \quad (5)$$

Eq. (5) is entered in Eq. (2) as model function to get the circuit parameter values. Fig. 7A shows the result of fitting the data in Fig. 4A between 15 MHz and 100 kHz using this equation. The best fitting parameter values are also given in the figure caption.

According to the model given in Fig. 5A, the dielectric capacitance, C_1, is associated to the solid-phase contribution. Taking into account the best fitting value for C_1 given in Fig. 7A (2.9 pF cm^{-2}), and considering the geometry of

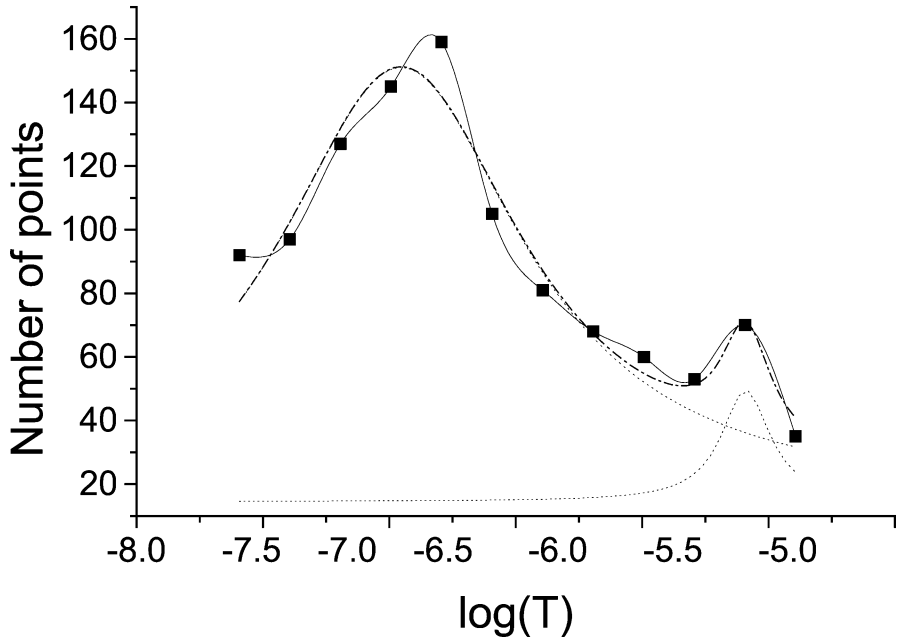

Fig. 6. Histogram resulting from application of DIA on data given in Fig. 4A in the frequency range 15 MHz to 100 kHz. Dotted lines correspond to the convolution of both peaks (see text).

the measurement given in Fig. 1A ($d = 0.4$ cm), from Eq. (6), a value of $\varepsilon = 13$ is obtained for this specimen.

$$\varepsilon = \frac{C_1 d}{\varepsilon_0} \tag{6}$$

In Eq. (6), C_1 is the calculated capacitance (F cm^{-2}), d is the sample thickness and ε_0 is the vacuum permittivity ($8.85 \cdot 10^{-14}$ F cm^{-1}).

Impedance measurements were performed also using the noncontacting method described in Fig. 1B. For this type of measurements, the impedance is capacitive (Fig. 4B, insert) in the frequency range 15 MHz down to 100 kHz, so it is reasonable to use a Cole–Cole representation instead of the complex plane impedance plot. Fig. 7B corresponds to the Cole–Cole of the impedance data given in Fig. 4B. These data have been modelled using the equivalent circuit given in Fig. 5B. The impedance for this circuit corresponds to Eq. (7) and its equivalent capacitance (Cole–Cole plot) to Eq. (8).

$$\frac{1}{Z(\omega)} = j\omega C_1 + \frac{j\omega C_2}{j\omega R_2 C_2} \tag{7}$$

$$C(\omega) = C_1 + \frac{C_2}{(1 + (j\omega R_2 C_2)^{\alpha})^{\beta}} \tag{8}$$

The transformation of Eq. (7) into Eq. (8) is evident. Eq. (8) has the advantage of showing two well-defined limits at high and low frequency in the complex plane capacitance plot (Fig. 7B), C_1 and $C_1 + C_2$, respectively. Additionally, it is easy to take account of the R_2C_2 time constant dispersion. The Havriliak–Negami formalism [23] has been employed for this purpose. The α and β parameters in Eq. (8) are constants, $0 < \alpha$, $\beta \leq 1$, that account respectively for the symmetric (Cole–Cole) and asymmetric (Cole–Davidson) dispersion of the R_2C_2 time constant. It is not the aim of this paper to discuss about the possible physical meaning of α and β parameters; thus, only their phenomenological aspect is considered.

Fig. 7B corresponds to the Cole–Cole plot corresponding to the impedance data given in the insert of Fig. 4B. The fitted data using Eq. (8) as model function are also given in the same figure, as well as the best fitting parameters (in the figure caption). If the obtained C_1 value (2.1 pF cm^{-2}) is entered in Eq. (6), a dielectric constant value $\varepsilon = 11.5$ is obtained for the system. Surprisingly, this value is lower than that obtained for the above discussed situation: the same sample and contacting measurement.

The self-consistency of C_1 determinations has been checked by systematic measurements on samples of varying thickness. The results are summarised in Fig. 8. As expected, according to Eq. (6), C_1 decreases as the specimen thickness increases so that the normalised value (dielectric constant) is independent on thickness for both types of measurements. However, the dielectric constant value obtained for the contacting measurement is significantly higher than for the noncontacting one (14 vs. 9 approximately). Thus, some kind of capacitance is added to C_1 when the driven electrodes touch the sample. If it was an interfacial effect, the resulting capacitance will be placed in series with C_1 and the measured value will result lower than

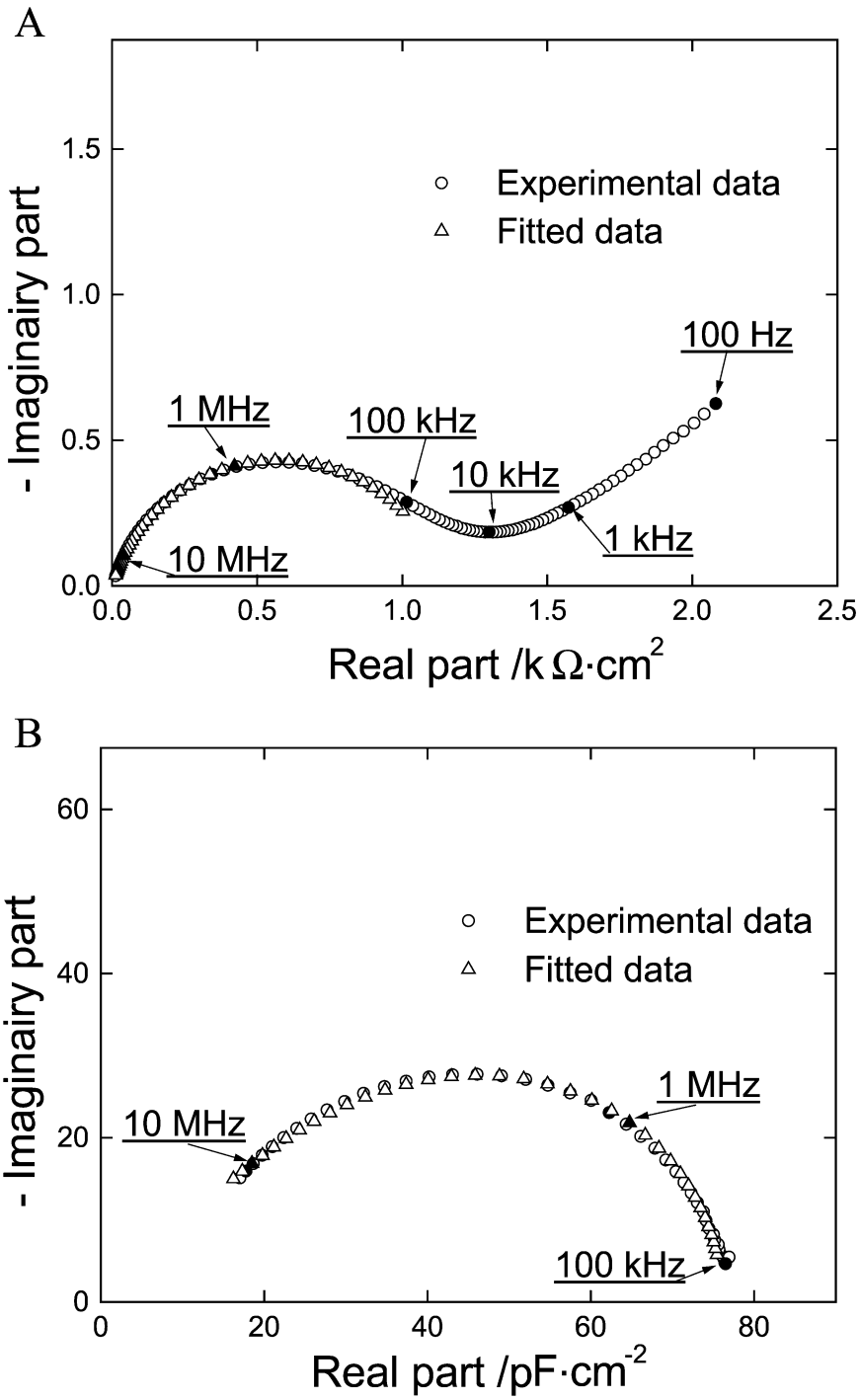

Fig. 7. (A) Complex plane impedance data given in Fig. 4A (contacting method) and fitted data for the frequency range 15 MHz to 100 kHz. Eq. (5) has been used as model function. The best fitting parameters are:

R_1, kΩ cm^2	C_1, pF cm^{-2}	α_1	R_2, Ω cm^2	C_2, pF cm^{-2}	α_2
18.6	2.9	1.0	153.6	2.2	0.76

(B) Cole–Cole plot corresponding to the impedance data given in Fig. 4B (noncontacting method). The experimental and fitted data in the frequency range 15 MHz to 100 kHz are given. Eq. (8) has been used as model function. The best fitting parameters are:

C_1, pF cm^{-2}	R_2, kΩ cm^2	C_2, pF cm^{-2}	α	β
2.1	1.6	2.2	0.83	1.0

the obtained in the noncontacting method. However, the stray capacitances due to border effects will be placed in parallel (and added) to C_1. Even if some additional experimental work is needed to verify this aspect, this contribution seems to be at the origin of the observed difference between the two types of measurements. The border effects are limited in the noncontacting method using a grounded guard ring while the contacting measurements are not guarded in the experimental set-up employed.

The consistency of C_1 determinations has also been checked with respect to the sample porosity. The results depicted in Fig. 9 have been performed using the noncontacting technique. Although the scatter in values is important, a linear dependence of the apparent dielectric constant with the w/c ratio is observed. The apparent dielectric constant decreases as the porosity of the sample increases (w/c ratio increases) so that a value of dielectric constant for the solid phase at zero porosity (w/c = 0) can be obtained, resulting $\varepsilon_{sp} \cong 16$. This value is consistent with that found in geo-radar studies at 0.1 GHz [24].

The dependence of C_1 (and thus ε) on the sample's porosity has already been reported elsewhere [5]. Although in that case, the data scattering was lower than that obtained here, in both cases, the scatter degree decreases as the mix workability increases (w/c ratio increases). It is also interesting to note that while a mechanical mixer was employed in the present study to prepare mixes, in the aforementioned paper [5], ultrasonic stirring was employed for mix homogenisation, which can explain the observed difference in data scattering.

4.4. The time constant R_2C_2. Influence of drying

According to the proposed model, the R_2C_2 time constant is associated to the ionic motion in the liquid phase thus, it is interesting to analyse the evolution of these parameters as the solvent in this dynamic phase is removed from the system.

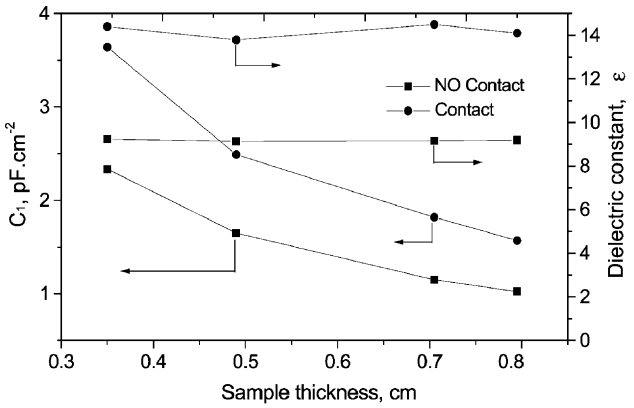

Fig. 8. Dependence of the C_1 parameter on sample thickness for contacting and noncontacting measures. Cement paste w/c = 0.5. The normalisation of C_1 with respect to the sample thickness gives a constant value for the sample dielectric constant, ε.

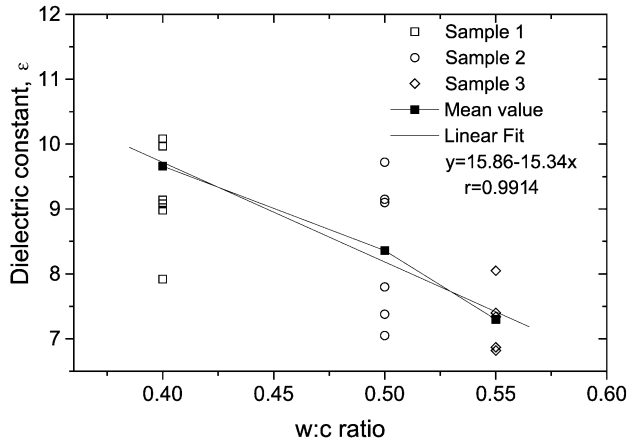

Fig. 9. Dependence of the apparent dielectric constant on w/c ratio. Measurements performed at 16 days curing using the noncontacting technique on six different samples for each w/c ratio.

The study was conducted on w/c ratio 0.4 samples cured for 50 days in 100% RH. The samples have been oven-dried at temperatures between 30 and 75 °C that allowed to perform IS measurements in a loss weight range up to 17%. Both contacting and noncontacting measurements have been performed.

Fig. 10 summarises the results obtained for the noncontacting method in the form of a Cole–Cole plot. It is interesting to note that the plot high-frequency limit does not depend on the water content in the sample, that is, C_1 accounts only for the solid phase, as discussed in the previous sections. Moreover, the low-frequency limit (C_2) seems to follow a random variation along the drying process.

The evolution of the model parameters C_1, C_2 and R_2 on drying is depicted in Fig. 11. The dielectric capacitance C_1 remains unchanged for all drying conditions, however, C_2 tends to increase as drying progresses and R_2 follows an almost exponential increasing path. The jagged C_2 increasing shows also a structure: the minimum values are roughly placed on two lines crossing at 12% drying (where R_2 starts increasing exponentially), and the first maximum approaches the value of the last minimum. The way for interpreting such behaviour is at least twofold:

(a) The capacitance C_2 can correspond to an electrostatic capacitance, C_{el}; associated to the moving charges needed to counterbalance the fixed charges in pore walls or CSH gel layers. This capacitance is concentration dependent (Eq. (9)) and then sensitive to the relative amount of water in the pores being dried.

$$C_{el} = \frac{\varepsilon\varepsilon_0}{L_D} \text{ being } L_D = \sqrt{\frac{\varepsilon\varepsilon_0 kT}{e^2 \sum z_i^2 c_i}} \quad (9)$$

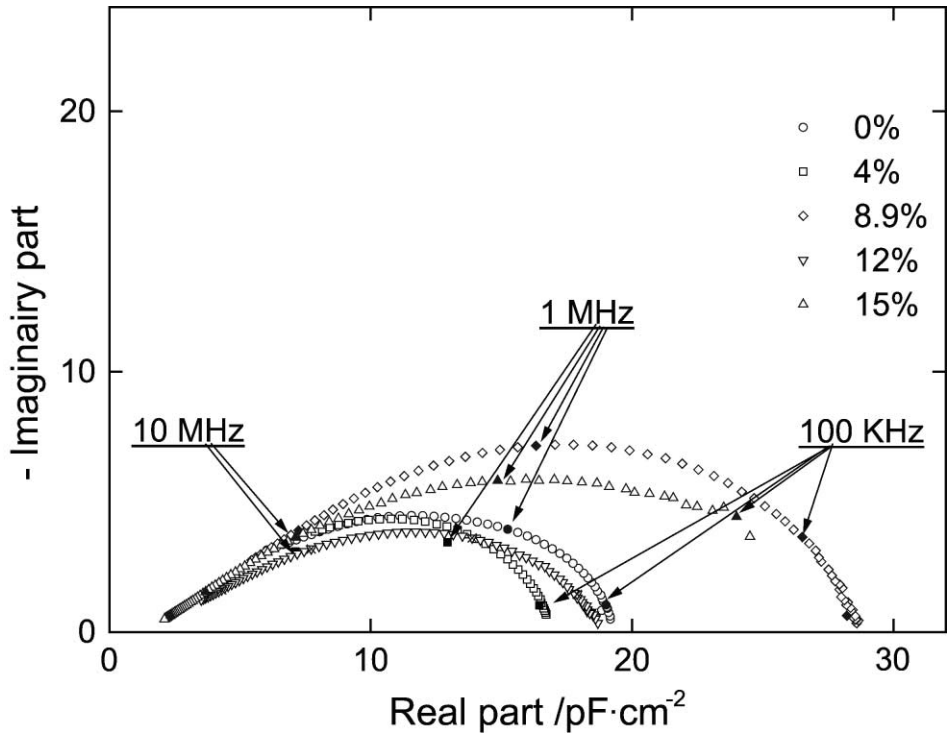

Fig. 10. Cole–Cole plots obtained for increasing drying (expressed as percent of weight loss). Sample: w/c ratio = 0.4, Thickness = 0.5 cm, 50 days curing at 100% RH.

L_D is the ionic Debye length and c_i the ion i concentration. As the sample dries out, the ionic concentrations increase and thus C_{el} increases. Of course, as the drying process is pore size dependent, the C_{el} variation will not be uniform at all.

(b) In addition to this electrostatic contribution to C_2, a chemical capacitance, C_{chem}, associated to stoichiometry changes, can be considered. This capacitance was defined in Ref. [25] and is placed in series to C_{el}, so the C_2 variation can also be understood as the transition from one dominant capacitance to the other one.

It is clear that the parameters C_2 and R_2 are directly related to the liquid phase/ionic motion in the paste pores, but further studies are needed to clarify the origin of C_2 capacitance.

Concerning the relationship between R_1 and R_2 in the model, some contacting measurements have been conducted. The results are presented in Fig. 12. Although R_1 is three orders of magnitude higher than R_2, both follow the same variation on drying, which also means that R_1 is related to the liquid phase (open pores contacting the driven electrodes).

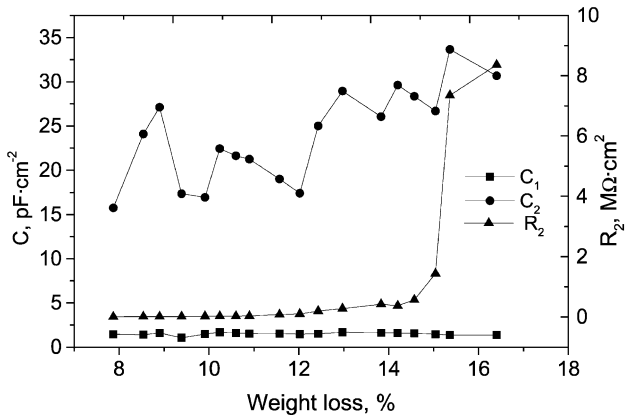

Fig. 11. Influence of drying (expressed as weight loss) on the model parameters values (noncontacting measurements). Parameters obtained from fitting of data given in Fig. 10.

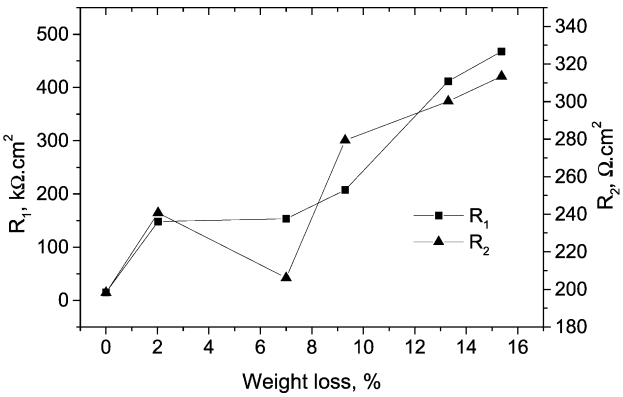

Fig. 12. Influence of drying (expressed as weight loss) on the variation of R_1 and R_2 parameters. Sample: w/c ratio = 0.4, Thickness = 0.5 cm, 50 days curing at 100% RH.

5. Conclusions

The differential impedance analysis was employed as a powerful technique to determine the number of the time constants present in an impedance spectroscopy plot. For hardened Portland cement paste, two time constants have been identified in the high-frequency impedance domain (100 kHz up to 40 MHz) even if only one apparent capacitive arch is observed in the complex plane impedance plot.

A measuring technique and a model to interpret IS results are presented. This procedure allows us to obtain the dielectric capacitance of cement paste free of contributions from the liquid phase, and thus opens the way for an electrical determination of porosity. A value of $\varepsilon \cong 16$ was extrapolated for zero porosity cement paste.

The ionic motion in the bulk electrolyte filling pores and interlamellar spaces is responsible for the R_2C_2 time constant. As R_2 and R_1 are parameters related to ionic mobility, it is expected that their study will allow gathering information related to diffusion mechanisms in concrete.

Acknowledgments

The authors thank the Spanish program DGICYT/FEDER for providing financial support to this research under project Ref. 1FD97-1161.

References

[1] W.J. McCarter, R. Brousseau, The a.c. response of hardened cement paste, Cem. Concr. Res. 20 (1990) 891–900.
[2] P. Gu, P. Xie, Y. Fu, J.J. Beaudoin, A.C. impedance phenomena in hydrating cement systems: Frequency dispersion angle and pore size distribution, Cem. Concr. Res. 24 (1994) 86–88.
[3] G. Levita, A. Marchetti, G. Gallone, A. Principallo, G.L. Guerrin, Electrical properties of fluidized Portland cement mixes in the early stage of hydration, Cem. Concr. Res. 30 (2000) 923–930.
[4] M. Keddam, H. Takenouti, X.R. Nóvoa, C. Andrade, C. Alonso, Impedance measurements on cement paste, Cem. Concr. Res. 27 (1997) 1191–1201.
[5] C. Andrade, V.M. Blanco, A. Collazo, M. Keddam, X.R. Nóvoa, H. Takenouti, Cement paste hardening process studied by impedance spectroscopy, Electrochim. Acta 44 (1999) 4313–4318.
[6] C. Andrade, L. Soler, X.R. Nóvoa, Advances in electrochemical impedance measurements in reinforced concrete, Mater. Sci. Forum 192–194 (1995) 843–856.
[7] B.J. Christensen, R.T. Coverdale, R.A. Olson, S.J. Ford, E.J. Garboczi, H.M. Jennings, T.O. Mason, Impedance spectroscopy of hydrating cement-based materials: measurement, interpretation, and application, J. Am. Ceram. Soc. 77 (1994) 2789–2804.
[8] R.T. Coverdale, B.J. Christensen, T.O. Mason, H.M. Jennings, E.J. Garboczi, Interpretation of the impedance spectroscopy of cement paste via computer modelling: Part II. Dielectric response, J. Mater. Sci. 29 (1994) 4984–4992.
[9] R.A. Olson, B.J. Christensen, R.T. Coverdale, S.J. Ford, G.M. Moss, H.M. Jennings, T.O. Mason, E.J. Garboczi, Interpretation of the impedance spectroscopy of cement paste via computer modelling: Part I. Bulk conductivity and offset resistance, J. Mater. Sci. 30 (1995) 712–719.
[10] R.A. Olson, B.J. Christensen, R.T. Coverdale, S.J. Ford, G.M. Moss, H.M. Jennings, T.O. Mason, E.J. Garboczi, Interpretation of the impedance spectroscopy of cement paste via computer modelling: Part III. Microstructural analysis of frozen cement paste, J. Mater. Sci. 30 (1995) 5078–5086.
[11] Goodfellow Catalogue 2000/2001. Goodfellow Cambridge, Huntingdon, England, 2000, pp. 412–415.
[12] C. Alonso, C. Andrade, M. Keddam, X.R. Nóvoa, H. Takenouti, Study of the dielectric characteristics of cement paste, Mater. Sci. Forum. 289–292 (1998) 15–28.
[13] Z. Stoynov, Structural spectral analysis of electrochemical impedance, Electrochim. Acta. 34 (1989) 1187–1989.
[14] D. Vladikova, Z. Stoynov, Conductivity mechanism of ytrium iron garnets investigated by differential impedance spectroscopy, Proc. of the Twenty-Seventh State-of-the-Art Program on Compound Semiconductors (Sotapocs XXVII), The Electrochemical Society Proceedings, vol. 97-21, The Electrochemical Society, Pennington, NJ, USA, 1997, pp. 242–250.
[15] D. Vladikova, Z. Stoynov, L. Ilkov, Differential impedance analysis on single crystal and polycrystalline Yttrium iron garnets, Pol. J. Chem. 71 (1997) 1196–1203.
[16] Z. Stoynov, Differential impedance analysis. An insight into the experimental data, Pol. J. Chem. 71 (1997) 1204–1210.
[17] J.R. Macdonald, in: J.R. Macdonald (Ed.), Impedance Spectroscopy Emphasizing Solid Materials and Systems, Wiley, New York, 1987, p. 274.
[18] M. Shi, Z. Chen, J. Sun, Kramers–Kroning transform used as stability criterion of concrete, Cem. Concr. Res. 29 (1999) 1685–1688.
[19] M.E. Orazem, J.M. Esteban, O.C. Moghissi, Practical applications of the Kramers–Kronig relations, Corrosion 47 (1991) 248–259.
[20] W.H. Press, B.P. Flannery, S.A. Teukolsly, W.T. Vetterling, Numerical recipes in Fortran, The Art of Scientific Computing, Cambridge University Press, Cambridge, U.K., 1986.
[21] Y. El Hafine, A. Smith, J.P. Bonnet, P. Abélard, P. Blanchart, Electrical characterization of aluminous cement at the early age in the 10Hz–1GHz frequency range, Cem. Concr. Res. 30 (2000) 1057–1062.
[22] J.R. Macdonald, in: J.R. Macdonald (Ed.), Impedance Spectroscopy Emphasizing Solid Materials and Systems, Wiley, New York, 1987, p. 96.
[23] S. Havriliak Jr., S.J. Havriliak, Dielectrical and Mechanical Relaxation in Materials, Hanser Publishers, Munich, Germany, 1997, p. 14.
[24] K Veness, Permitivity measurements and analytical dielectric modelling of plain structural concretes, 7th International Conference on Ground Penetrating Radar, Kansas. The University of Kansas, Lawrence, Kansas, USA, 1998, pp. 363–368.
[25] J. Jamnik, J. Maier, S. Pejovnik, A powerful electrical network model for the impedance of mixed conductors, Electrochim. Acta 44 (1999) 4139–4545.